Available online at www.sciencedirect.com
SCIENCE DIRECT®
Journal of Non-Crystalline Solids 352 (2006) 567–577
JOURNAL OF NON-CRYSTALLINE SOLIDS
www.elsevier.com/locate/jnoncrysol

Mass transport in chalcogenide electrolyte films – materials and applications

Michael N. Kozicki, Maria Mitkova *

Center for Solid State Electronics Research, Arizona State University, P.O. Box 6206, Tempe, AZ 85287-6206, USA

Available online 20 March 2006

Abstract

Certain metals can be added to thin films of chalcogenide glasses by photodissolution to create materials with unique morphology and properties. When Ag is combined in this fashion with Ge–Se or Ge–S glasses, the resulting ternary contains a dispersed nanocrystalline Ag_2S(e) phase that has large quantities of mobile metal ions. The presence of these ions allows the ternaries to act as solid electrolytes. If an anode which has an oxidizable form of the ionic metal and an inert cathode are applied in contact with such a phase-separated electrolyte, an ion current can flow under an applied bias in excess of a few hundred millivolt. Electrons from the cathode reduce the excess metal due to the ion flux and an electrodeposit forms on or in the electrolyte. Utilizing this effect, we developed programmable metallization cell (PMC) technology which offers new functionality for such materials. Based on mass transport driven by electrochemical processes, PMC technology may be applied in solid state electronics, integrated optics, microelectromechanical systems (MEMS), and microfluidics. This paper is a review of the unique materials aspects of thin film solid electrolytes formed by photodissolution of metal into a chalcogenide base glass and the demonstrated applications of this technology.

PACS: 61.43.Fs; 61.82.Rx; 66.10.Ed; 66.20.Dn

Keywords: Amorphous semiconductors

1. Introduction

Deposition electrochemistry has been an important part of the microelectronics industry for many years. For example, electroplating has been utilized in integrated circuit packaging for decades and more recently in the processes used to make Cu wiring within the chips. Electrochemistry deals with the relationship between electricity and chemical change. Electrons removed from atoms in the process of oxidation create ions and these charged species are able to move under the influence of an electric field in liquid or *solid* electrolytes. On receiving an electron, a displaced ion is reduced and becomes an atom. In this situation, the net change brought about by electrochemistry is the *redistribution of mass* – the atoms are removed from one location and are deposited in another with ion transport in the electrolyte occurring in between. An ion current will only occur in an electrolyte if an oxidizable electrode (the anode) is made positive with respect to an opposing electrode (the cathode) and sufficient bias is applied, typically greater than a few hundred millivolts [1]. The voltage threshold effect is a result of the underlying electrochemistry in that electrodeposition will only occur if the applied voltage is sufficient to overcome the chemical potential barrier at the electrode. The number of atoms moved and deposited will correspond to the number of electrons that take part in the process and these are supplied by the external circuit. The electrodeposited mass is therefore controlled by the total *Faradaic* charge (which takes part in the electrochemical reaction) from the power supply [2]. Each metal ion undergoing reduction is balanced by a metal atom becoming oxidized and this avoids the

* Corresponding author. Tel.: +1 480 965 9481; fax: +1 480 965 8118.
E-mail address: mmitkova@asu.edu (M. Mitkova).

0022-3093/$ - see front matter © 2006 Elsevier B.V. All rights reserved.
doi:10.1016/j.jnoncrysol.2005.11.065

formation of an internal electric field due to the build up of charge which would ultimately cancel the applied field and stop the electrodeposition. Note that if the opposite electrode is electrochemically inert (not oxidizable), the electrodeposition process is reversible by much the same rules that govern growth except that we must reverse the polarity of the applied bias. When the electrodeposit is made positive with respect to the original oxidizable electrode, it becomes the new anode and will dissolve via oxidation. During the dissolution of the electrodeposit, the balance is maintained by deposition of metal back onto the electrode where the excess metal for the electrodeposition came from in the first place. Once the electrodeposit has been completely dissolved, the process self-terminates. It is important to note that it is the *asymmetry* of the structure that allows the deposition/dissolution process to be cycled repeatedly.

The ability to redistribute metal mass within a structure in situ via the application of a voltage leads to a wide range of potential applications. Electrodeposition of a noble metal such as Ag produces localized *persistent* but *reversible* changes to materials parameters and these changes can be used to control system behavior. For example, deposition of mass can be used to decrease the resonant frequency of a vibrating element in a microelectromechanical system (MEMS) [3]. The optical properties of the electrodeposits will obviously have a profound effect on the transmission and reflection of light and so optical switches become a possibility using this technique [4]. Of course, electrical resistance will change radically when an electrodeposit with a resistivity in the tens of μΩ cm or lower is deposited on or in a solid electrolyte which has a resistivity some eight orders of magnitude higher; this leads to a myriad of applications in solid state electronics [5,6]. Finally, and perhaps most astonishingly, the morphology of a typical electrodeposit leads to a large change in the wetting of a surface, making it highly hydrophobic, and so the technique could also be used in microvalves and other fluid/droplet control devices [7]. We have demonstrated all of these effects and summarize our results in this review to illustrate how new functionality of ionic glasses can be achieved using mass transport in solid electrolyte films.

2. Solid electrolyte structure

A variety of inorganic and organic materials can conduct ions to some extent but we typically focus in the context of electrochemical mass-transport devices on compounds of oxygen (O_2), sulfur (S), and selenium (Se), principally because of their ability to withstand processing at elevated temperatures and high ion mobility at normal device operating temperatures. Combining these with copper (Cu) or silver (Ag) gives us binary electrolytes such as Ag_2S [8] or Cu_2S [9]. Alternatively, we can react a transition metal such as tungsten (W) with oxygen to form the type of solid electrolyte that has been used in electrochromic devices [10]. Yet another approach is to combine chalcogens with other elements such as germanium to form a base glass into which we can dissolve Cu or Ag. An example of a ternary electrolyte formed this way is $Ag_{0.33}Ge_{0.20}Se_{0.47}$ [11], which is essentially a glassy Ge-rich backbone mixed with an Ag_2Se phase in the form of dispersed nanoscale *superionic* regions. The distinctive nanostructure of this material and its sulfide counterpart leads to a highly stable solid electrolyte that has high ion mobility (as much as 10^{-3} cm^2/V s) even though its resistivity is relatively large (100 Ω cm or greater) [12]. The Ag–Ge–Se and Ag–Ge–S ternaries are of greatest interest to us in our work as they are easy to form as thin films on devices and they exhibit good thermal stability in subsequent processing and during device operation. In our experience, the selenide electrolytes, which exhibit the highest ion mobility, are completely stable at processing temperatures up to 200 °C and operating temperatures as high as 110 °C whereas the sulfide variants are capable of withstanding processing temperatures beyond 400 °C and will operate above 150 °C without damage. The main drawbacks of sulfide electrolytes is that the ion mobility is around a factor of 10 lower than that in the selenide ternaries and film stoichiometry is more difficult to control due to the high vapor pressure difference between Ge and S. Both these electrolytes support fast electrodeposition growth rates and Ag is relatively inert.

Extensive studies on the materials aspects of the ternary systems of interest have been performed [13–15]. The nature of glass formation was first established in the Ag–Ge–Se glass system [13,14] and later investigated in Ag–Ge–S glasses [15]. Using direct techniques such as modulated differential scanning calorimetry (MDSC), Raman spectroscopy, and Mössbauer spectroscopy, it was found that the materials are phase separated for the case of chalcogen-rich ternaries in both systems and that Ag can replace a portion of Ge in Ge-rich compounds.

The amount of Ag that can be introduced into the chalcogenide film due to photodissolution is larger than in the case of bulk glasses and Ag incorporation is self-limiting [16]. We assume that the Ag concentration reaches saturation because of the limited number of free and under-coordinated Se atoms that are available for reaction with Ag to form the Ag_2Se phase as described in [11].

Two approaches were used for the characterization of the diffusion products; (1) Raman spectroscopy, giving information about the evolution of the Ge-chalcogen backbone following diffusion which remains amorphous, and (2) X-ray diffraction (XRD), to give information on the Ag-containing products which turn out to be nanocrystalline. In our studies of the Ag–Ge–Se system in bulk or thin film form, we have always found Ag chemically bonded. This fact has the important consequence that some Se is extracted from the initial Ge–Se backbone to react with the diffused Ag. Thus, after chemical interaction the remaining chalcogenide glass backbone becomes Se deficient, yielding a Raman signature characteristic of Ge-rich glass that is independent of the initial composition of the host and its initial Raman scattering (Fig. 1). Following

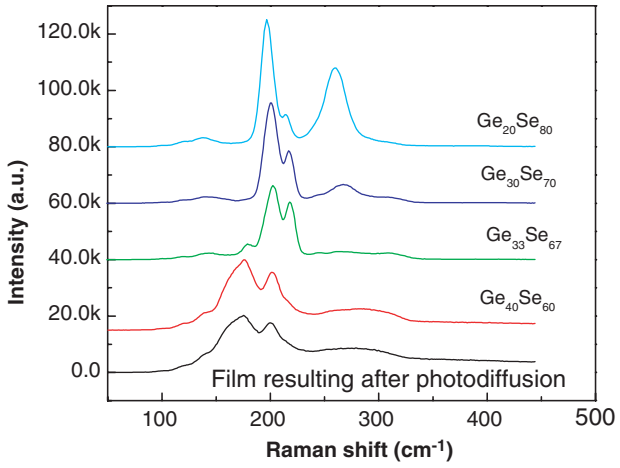

Fig. 1. Raman spectra of undoped Ge–Se thin films of various compositions and the spectrum of the material after Ag photodissolution.

diffusion, the underlying molecular phase consists of face-sharing quasi one-dimensional ethane-like $Ge_2(Se_{1/2})_6$ chain fragments whose presence is manifested on the Raman spectra by the appearance of the mode at 180 cm^{-1} [18] depicted in Fig. 1. The Raman spectrum of the resulting material shows a lower intensity ratio between the modes at 180 cm^{-1} and the mode of the Ge-tetrahedral units at 200 cm^{-1} compared to the intensity ratio of these modes for a $Ge_{40}Se_{60}$ glass film. This is an indication that the number of ethane-like units is lower than in $Ge_{40}Se_{60}$ glass. This is a result of the spontaneous reaction of Ag with some charged metastable states on the chalcogen [17] initiated by light illumination and with charged defects occurring at bond conversion [19]. The structure of the Ge–Se backbone formed after photodoping is depolymerized to some extent due to the extraction of Se and formation of crystalline products. Because of this and the high stiffness of the backbone, the organization of the photodiffused glass does not change with low temperature annealing. This is different from the case of pure Ge–Se films [20] where the local stressed configurations with high free energy relax through breaking the Ge–Ge bonds and the formation of Ge–Se corner-sharing units due to reaction with some Se–Se wrong bonds occurs.

The form in which Ag is included in the system was inferred from XRD analysis since the diffusion product occurs in a nanocrystalline form. XRD revealed a close dependence of the diffusion product composition on the composition of the host. Diffractions from both β-Ag_2Se (orthorhombic) and α-Ag_2Se (cubic) phases [21] were observed following diffusion of Ag in $Ge_{20}Se_{80}$ glass – Fig. 2(a), while in a more Ge-rich host, formation of Ag_8GeSe_6 takes place. An example of the Ag diffusion products for the case of a $Ge_{33}Se_{67}$ base glass is given in Fig. 2(b). The unexpected presence of the high-temperature cubic form of Ag_2Se revealed by this study could be due to volume restrictions as the Ag_2Se forms during Ag photodiffusion in the existing solid-state framework of the Ge–

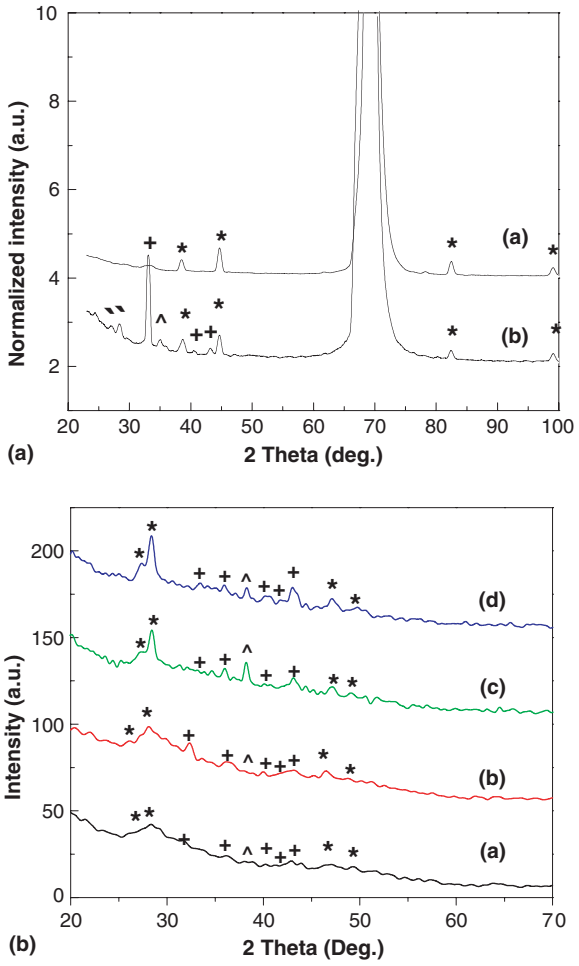

Fig. 2. XRD spectra of thin chalcogenide films photodiffused with Ag. (a) Initial host composition $Ge_{20}Se_{80}$ covered with Ag (a) and same film after Ag diffusion (b); ∗ peaks of Ag; ∧ peaks of αAg_2Se; + peaks of βAg_2Se. (b) $Ge_{33}Se_{67}$ doped with Ag and annealed at: (a) 85 °C for 15 min, (b) 85 °C for 120 min, (c) 150 °C for 15 min and (d) 150 °C for 120 min; ∗ peaks of Ag_8GeSe_6; ∧ peaks of αAg_2Se; + peaks of βAg_2Se.

Se backbone. The orthorhombic phase that is stable at room temperature has a more loosely packed structure than the cubic form and we suggest that the surrounding hosting glass restricts its expansion. Although a number of floppy units are available in the initial structure of the host, with the first inclusion of Ag and formation of Ag_2Se the structure becomes stiffer since it is depleted in selenium. So the internal space limitation acts in the same way as elevated pressure, stabilizing some clusters in the high-temperature cubic form of Ag_2Se which has the closest packing.

One major part of our research on ternary solid electrolytes addresses the issue of crystal size of the diffusion products and how this factor depends on the hosting material and on annealing at temperatures up to 150 °C. The XRD spectra were taken at room temperature and the Scherrer equation was used to estimate the particle size of the small crystals from the measured parameters of their diffraction peaks using the broadening at half the peak height by

$$t = (0.9\lambda)/B\cos\theta, \quad (1)$$

where t is crystallite size, λ is X-ray wavelength, B is the full width at half maximum of the peak, and θ is the angle at full width of half maximum. There is a clear tendency for the nanocrystals to become larger with Ge content of the host, becoming largest when the Ag is introduced into a $GeSe_2$ glass, and subsequently decreasing in size for higher Ge concentration. Fig. 3(a) and (b) illustrate the dependence of crystal size on composition and annealing conditions for $Ge_{10.5}Se_{42.3}Ag_{47.2}$ and $Ge_{22.1}Se_{44.9}Ag_{33}$ glasses. We suggest that this effect is related to the molecular clustering of the hosting glass. As noted by Feltz et al. [22] the evolution of molar volume with composition in Ge_xSe_{1-x} system has a maximum at $x = 0.33$, i.e., for $GeSe_2$ where the structure is less densified. The data collected by Feng et al. [23] confirm same structural evolution. Furthermore, there is evidence for the importance of the structural characteristics of the host and rigidity percolation in it [24]. Although the lattice parameters of Ag_2Se are smaller, in the cases when Ag_8GeSe_6 crystallizes in a more rigid backbone its initial clusters are smaller than the Ag_2Se clusters in a structure with a larger free volume and higher flexibility of the host.

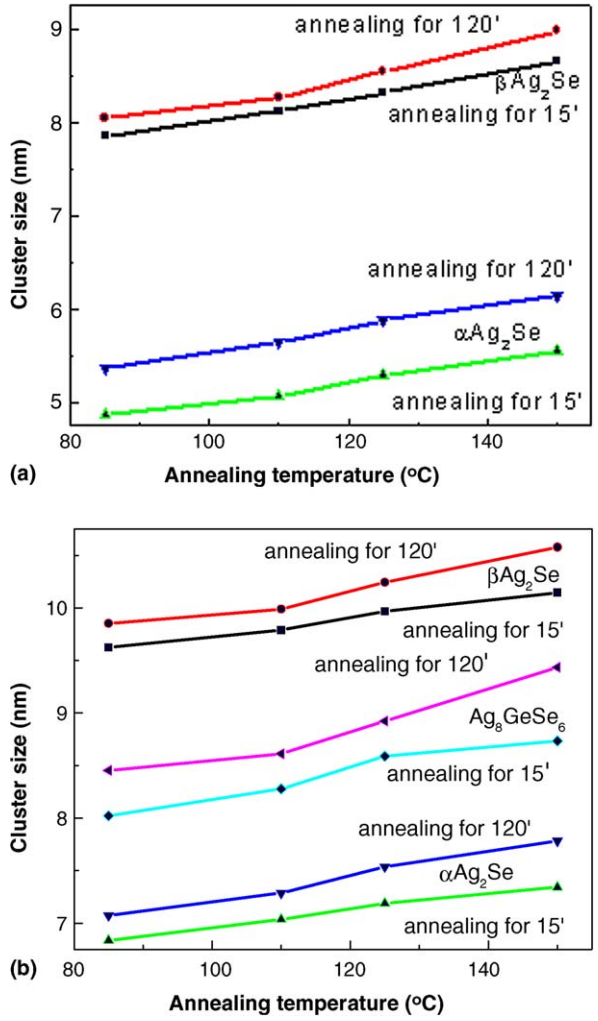

Fig. 3. Size of different clusters found in annealed glasses with compositions: (a) $Ge_{10.5}Se_{42.3}Ag_{47.2}$ at the conditions shown in the figure. (b) $Ge_{22.1}Se_{44.9}Ag_{33}$ at the conditions shown in the figure.

A final point of interest is the development of crystal growth at elevated temperatures. The conditions discussed in this work are relatively mild since our ultimate goal is to deduce information useful for the high-temperature processing of these materials. The extended anneal resulted in no observable change in the composition of the crystalline products with time at the chosen temperatures. In the case of the Ag_2Se clusters, the crystalline phases are different from the surrounding material and we assume that their growth is limited by atomic diffusion (to about 5–8% after annealing), which is restricted due to the heterogeneous character of the medium. In the case of formation of Ag_8GeSe_6 clusters, the growth is much more affected by the annealing and their size changes by about 8–10%. This situation closely corresponds to homogeneous growth. We suggest that the adjacent clusters fuse with Ge atoms cross-linking the cluster edges and leading to formation of a common structure combining the three elements.

We can estimate the distance, s, between the Ag_2Se crystallites in the chalcogen-rich materials and therefore the thickness of Ge-rich material between them by assuming that these regions are spherical and uniform in size and dispersion, so that

$$s = d(F_v^{-1/3} - 1), \quad (2)$$

where d is the measured diameter of the crystalline Ag-rich phase and F_v is the volume fraction of this phase. Since the volume fraction of Ag_2Se in $Ag_{33}Ge_{20}Se_{47}$ is 0.57 (for a molar fraction of 0.63), the average spacing between the Ag-rich regions is 0.2 times their diameter. So, for an average Ag_2Se crystallite diameter of 7.5 nm, we can expect an average separation of 1.5 nm. As we will see in Section 5 of this paper, this unique nanostructure is critical to the electrical characteristics of the electrolyte film. Here the ion-containing mixed conductor crystallites dominate the composition and the films appear superionic, but the Ge-rich material in the interstices ensures that the film resistivity is relatively high.

3. Solid electrolyte formation

Our ternary electrolytes are typically formed in a two step process in which a binary (Ge–Se or Ge–S) base glass is deposited first and then capped with a thin Ag film, the two layers being combined by photodissolution. The Ge content of the binary ranges from 20 to 40 at.%, the exact choice being dependent on the electrodeposit morphology required (discussed later in this paper).

Photodiffusion from a thin surface film using ultraviolet light is a relatively simple way to add Ag to a binary base glass at low temperature to form a uniform ternary electrolyte in a highly controlled manner [25,26]. The process of photodissolution is driven by the formation of optically

induced charged defects in the chalcogenide glass which create an electric field. The light energy that drives the photodissolution is absorbed at or near the interface between the reacted and unreacted chalcogenide layer [27,28]. In this process, the holes are trapped by Ag, while electrons are shifted deeper into the chalcogenide film and trapped there. The Ag species move in the doped chalcogenides as positively charged ions [29,30]. The electric field formed by the negatively charged chalcogen atoms and positively charged Ag^+ ions is sufficient for them to overcome the energy barrier at the interface. So, the penetration of the metal into the chalcogenide during photodoping is actually due to the difference in electrochemical potentials. We can consider the process to be similar to that occurring in a galvanic cell, in which case the more electropositive metal is dissolved into the electrolyte due to an intercalation reaction [31,32]. The main reason that this reaction occurs in chalcogenide glasses is that they possess relatively rigid covalent bonds mixed with soft van der Waals interconnections. This type of structure ensures the formation of voids and channels where the diffusing ions can migrate and be hosted.

The dissolution process described above results in the formation of bonds with the host matrix according to the reaction

$$C_2^0 + e^- + Ag^+ \rightarrow C_1^- Ag^+ \quad (3)$$

which describes the transition of an initially twofold covalently bonded chalcogenide atom (C_2^0) into a C_1^- charged unit. This latter specie possesses only a single covalent bond and an excess electron that establishes an *ionic* bond with the Ag^+. The equation above shows the importance of the new C_1^- Ag^+ bonds in the intercalation product. The possible number of these bond-units is high as chalcogenide glasses are uniquely capable of forming a large number of single C_1^- centers under appropriate illumination. This not only allows photodissolution to proceed so readily but also results in the necessary structure for the solid electrolyte in which plentiful Ag^+ ions are weakly held at a large number of negatively charged chalcogen sites. The ions easily move from site to site under the influence of an electric field and so the ion mobility is relatively high.

In our photodissolution process we typically use a UV source wavelength of 405 nm and power density around 5 mW/cm^2 for a minimum of 10 min. The thickness of Ag film is kept to less than 25 nm to allow sufficient light to penetrate to the interface to stimulate the photodissolution process in a reasonable amount of time. Saturation of the base glass occurs when the diffusing Ag^+ ions react with all available chalcogen atoms as discussed in the previous section and so the concentration of Ag at saturation actually depends on the amount of chalcogen in the base glass, reaching 47 at.% for a base glass with 80 at.% chalcogen [11]. Our data from Auger electron spectroscopy (AES) reveals that illumination using the minimum time causes penetration of the diffused Ag into the base glass to a depth of approximately 40 nm (see Fig. 4 for an example of a Ag photodiffusion into a 50 nm thick film). If the photodissolution time is long (>10 min) so that the photodissolution process is driven to completion, a 20 nm thick Ag film will completely saturate a 50 nm thick film of base glass, leaving an extremely thin and typically discontinuous metallic Ag film on the surface which can be removed using $Fe(NO_3)_3$ solution. To avoid the excess Ag etching step, a thicker base glass film (e.g., 80 nm) could be used with a 15–20 nm silver film so that all Ag is driven from the surface but the entire film thickness would not be silver saturated in this case.

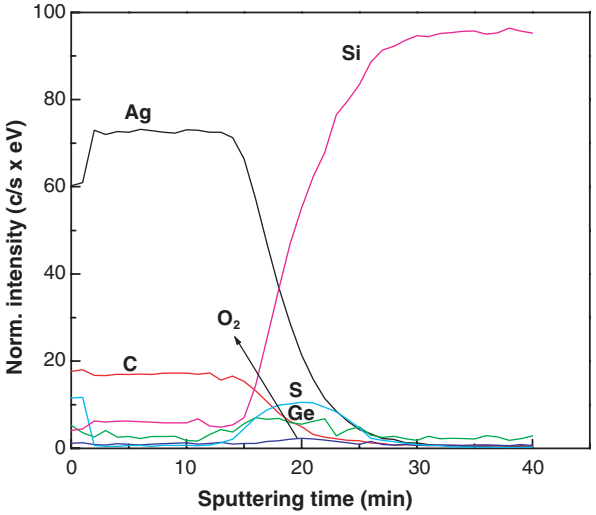

Fig. 4. AES determination of the relative change of the atomic concentration in $Ge_{22}S_{78}$:Ag after photoinduced diffusion; film profile on silicon substrate as a function of sputtering time.

4. Electrochemical processes

As can be seen from the discussion on the nature of the electrolyte above, only the positively charged ions are able to move and the negative charge centers are fixed in the electrolyte. This means that a charge imbalance (and associated electric field) will arise if reduced ions are not replaced by the oxidation of metal at the anode which underscores the need for oxidizable metal at this electrode. Electrodeposition also requires an applied bias above a particular threshold to overcome the effects of the cathodic barrier. The intrinsic potential difference necessary to do this is typically only a few hundred millivolt and this must be dropped across the polarized double layer at the cathode. The specific resistance of the polarized region is in the order of 10^{10} Ω μm^2 [1].

The ions nearest the electron-supplying cathode will be reduced first. Statistical non-uniformities in the ion concentration and in the topography of the electrode will tend to promote localized deposition or nucleation rather than blanket plating on the cathode. However, even if multiple nuclei are formed, the one with the highest field and best ion supply will be favored for subsequent growth, extending out from the cathode as a single metallic feature. The

electrodeposition of metal on the cathode does not mean that ions entering from the oxidizable anode have to travel the entire length of the structure to replace those that are reduced. The ion closest to the reduced ion will move to the vacated negative site on the hosting material and those upstream will do likewise, each filling the vacated site of the one downstream, until the last vacated space closest to the anode is filled by the incoming ion. So the ion current is actually a ripple effect, known in electrochemistry as a *coordinated motion*. Since the electrodeposit is physically connected to the cathode, it can supply electrons for subsequent ion reduction. So the growing electrodeposit will harvest ions from the electrolyte, plating them onto its surface to extend itself outwards from the cathode. This can lead to electrodeposits that are several hundred microns in length. Since each ion deposited on the growing electrodeposit corresponds to one that has been removed from the metal source, the net effect is a shift of mass from the anode to the cathode, even though in the initial stages, the electrodeposit is actually made up of reduced ions from the electrolyte itself.

Interestingly, even though we strive to create electrolytes with the highest possible ion mobilities, it frequently is not the mobility that is the growth rate limiting process. The growth occurs at the cathode double layer and this is typically only a few tens of nanometer wide so a few hundred millivolt will create a field of 10^5 V/cm. This leads to an effective ion velocity of 1 m/s if the mobility is 10^{-3} cm^2/V s. We can expect the ions to arrive at the growing electrodeposit from the surrounding electrolyte at this rate, adding to it to propel its growth forward at a considerable velocity. Clearly, a higher applied voltage would drive more current and this would increase the growth rate but there is the danger of exceeding the breakdown voltage of the surrounding dielectric (as well as transcending practical operating limits of the system) if we go too high. The key is therefore to balance factors such as device dimensions and electrodeposit mass/volume with operational requirements such as speed and control voltage.

The general nature of the morphology of the electrodeposits that form on the surface of the solid electrolytes corresponds to those reported for diffusion-controlled processes such as diffusion-limited aggregation (DLA) [2]. However, we were the first to note that the composition of the solid electrolyte had a profound effect on the morphology of these deposits [4]. It is likely that the nucleation points from which the electrodeposits grow are related to the presence of excess Ag ions on the electrolyte surface as the free energy for electrodeposit formation in these regions will be lowest. In the case of $Ge_{20}Se_{80}$ glasses, the glass structure is floppy [33] and the illumination with light will likely cause considerable depolymerization of the Se chains [27]. As a result, a number of randomly distributed charge defects can occur with which the photodiffused Ag reacts to form substantial Ag_2Se regions which act as nuclei for the formation of electrodeposits. This, coupled with the high Ag content of these films, is the reason that we observe a great number of distributed Ag electrodeposits with microscale to nanoscale dimensions covering the surface of the films, as shown in the atomic force microscope image of Fig. 5(a). In the case of the Ge-rich glasses ($Ge_{40}Se_{60}$), we assume that Ag-containing units that serve as nucleation centers exist in the volume and surface of the film as three component structural units, similar to those present in bulk material [13] in which Ag replaces Ge in the building blocks with distorted rock salt structure. The occurrence of similar exchange reaction that forms Ag-containing three component structural units following Ag diffusion has been observed in As_2S_3 films [34]. The formation of this structure will lead to regions of material that have significantly different conductivity [35]. The result is growth of 'isolated' much larger electrodeposits [4] as illustrated in Fig. 5(b).

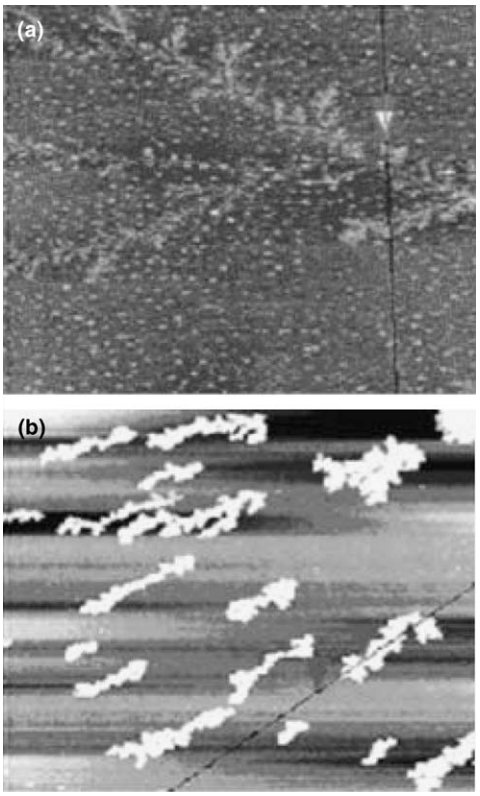

Fig. 5. Atomic force microscope (AFM) analysis (3D topographical scan) of Ag electrodeposit grown on (a) Ag-saturated $Ge_{20}Se_{80}$. The growth is continuous and the maximum electrodeposit height is a few tens of nanometer; (b) Ag-saturated $Ge_{40}Se_{60}$. The growth appears discontinuous and the maximum electrodeposit height is in the order of 100 nm.

5. Applications of mass transport in solid electrolytes

5.1. Patterning of the electrolyte

We have described the materials characteristics and formation techniques for the solid electrolytes in the previous sections but in order to apply them to devices and systems, they must be able to be patterned. Fortunately, a number of options exist for the patterning of the electrolyte layer.

The simplest method is lift-off, in which the photoresist is spun-on, exposed using an optical printer/aligner, and developed *prior* to electrolyte deposition so that subsequent solvent removal of the resist leaves only the electrolyte in the developed regions. The other subtractive alternative is to pattern the resist after base glass/silver deposition and use wet chemical or dry etching to remove the areas not covered by resist. This should be done prior to photodissolution as it is easier to etch the bilayer than the ternary. For example, in wet etching, the Ag layer can be etched with $Fe(NO_3)_3$ while the base glass will be etched with basic solutions in which the pH is adjusted using phosphates as pointed out in [5,36]. In the case of dry etching, a physical etch with Ar^+ or CF_3^+ can sputter away the thin silver and a CF_4/O_2 chemical etch will remove the base glass – both may be performed in a reactive ion etch system. The third alternative is to use the photodissolution step itself to define the pattern in the electrolyte and remove the unexposed regions using wet or dry chemistry, the ternary being relatively insoluble in the etchants used to remove the bilayer [37]. The main advantage of this latter approach is that no photoresist is required.

Two major categories of solid electrolyte devices have been investigated – lateral and vertical structures. In the lateral structures, the electrodes are coplanar on the surface of the electrolyte and the electrodeposit forms between them on the surface of the film. For the vertical devices, the thin film of electrolyte is placed between the electrodes so that the electrodeposition is forced to occur within the glass. As we will see later in this section, the lateral arrangement is utilized when large electrodeposits are required to alter the physical properties of a surface, whereas the vertical structure is best suited to fast electrical switching as the distance between the electrodes is governed by the electrolyte film thickness and this can be in the order of tens of nanometer or less.

5.2. Solid state memory

One of the most significant applications of mass transport in solid electrolytes to date has been in programmable metallization cell (PMC) memory [38,39]. The PMC memory device, illustrated in Fig. 6, is a vertical structure, comprising of a thin film (typically 50 nm or less in thickness) of Ag- or Cu-based solid electrolyte sandwiched between a Ag or Cu anode respectively and an electrochemically inert cathode (e.g., tungsten). Electrodeposition in the electrolyte, rather than on its surface, switches the device from a high resistance state to a value many orders of magnitude lower. The low series resistance of the thin film means that the electrodeposition occurs at the lowest possible voltage – a few hundred millivolt – and the small distance between the electrodes allows rapid switching for small quantities of electrodeposited material and applied charge. The asymmetry of the structure allows cycling of the device between non-volatile high and low resistance states, so they may be used as switching/resistance change elements in memory and logic circuits. The structure is highly scalable and devices as small as 40 nm in diameter have been demonstrated [5].

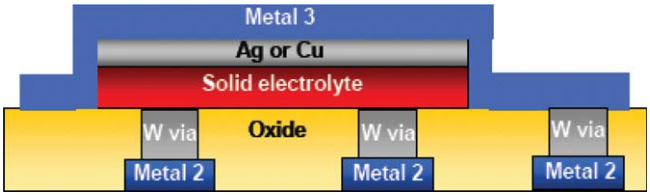

Fig. 6. Cross sectional schematic of a vertical PMC memory structure. In this scheme, the solid electrolyte layer is sandwiched between individual tungsten plugs and a continuous Ag or Cu layer in the upper levels of metallization in an integrated circuit.

Although no direct evidence exists for the exact nature of the electrodeposition process within the electrolytes, it is reasonable to assume that electrodeposition will initially occur in the high resistivity ($>10^6\,\Omega\,cm$) Ge-rich regions where the local electric field is highest. The bridging of these regions will occur until the resistance of the bridges is equivalent to that of the crystallites and the electrodeposition will then likely occur along the length of the pathway. Note that if the overall resistance of the conducting pathway is dominated by the resistivity of the Ag_2Se regions, which is in the order of $2\times10^{-3}\,\Omega\,cm$, an on resistance in the order of $10^4\,\Omega$ will require a conducting region of only 20 nm in diameter. The small size of the conducting pathway in comparison to the device area explains why on resistance has been observed to be independent of device diameter, whereas off resistance increases with decreasing area [6]. Lower resistance is possible once the pathway becomes predominantly metallic but the low resistivity of the metal (in the order of $10^{-6}\,\Omega\,cm$) means that the diameter of the conducting pathway is not much larger than 20 nm even for an on resistance below 1 kΩ. During electrodeposition, when the device resistance falls to the point where a current-limited voltage source creates insufficient voltage drop across the device to support further metal deposition, the process will halt. The on resistance, R_{on}, is therefore determined by

$$R_{on} = V_{te}/I_{prog}, \tag{4}$$

where V_{te} is the minimum voltage required to sustain electrodeposition once the process has started (typically between 100 and 200 mV) and I_{prog} is the current limit of the external voltage source. It is therefore possible to control the end point of the electrodeposition process and, therefore, the on resistance using programming current.

Fig. 7 gives representative resistance–voltage characteristics of 32 consecutive voltage sweeps of −0.5 to +0.5 to −0.5 V with a 10 μA current limit on a 75 nm diameter PMC memory device. The device switches from over $10^7\,\Omega$ to its low resistance state of $10^4\,\Omega$ at around 0.2 V and the conducting pathway breaks at −0.04 V [5].

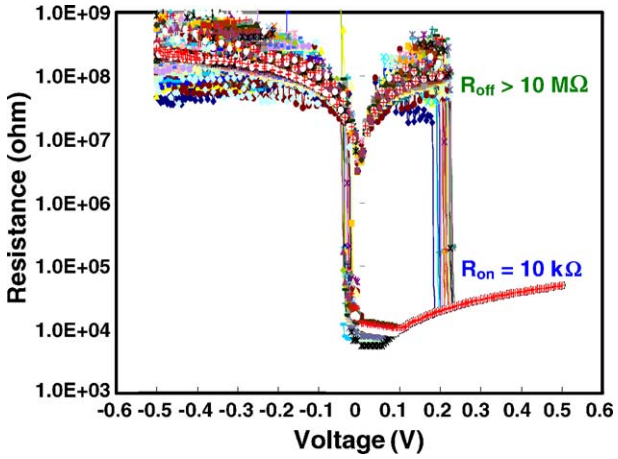

Fig. 7. Resistance–voltage plot from a 75 nm Ag–Ge–Se device using 32 voltage sweeps of −0.5 to +0.5 to −0.5 V with a 10 μA current limit. The device switches from over 10^7 Ω to its low resistance state of 10^4 Ω around 0.2 V and the conducting pathway breaks at −0.04 V.

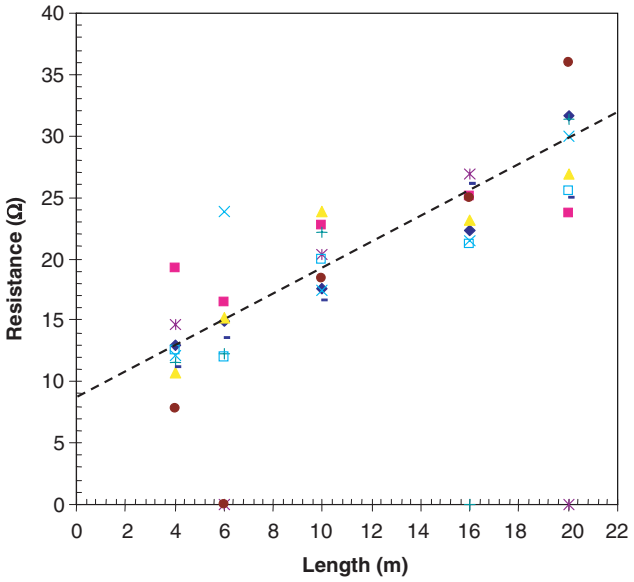

Fig. 8. Programmed resistance vs. length (10 μm wide) for a 25 mA current limit; different symbols represent data from different device samples.

5.3. Programmable wiring

Silver electrodeposition can vastly alter the electrical resistance of the surface of a structure. Given the eight orders of magnitude difference in resistivity between the electrolyte and thin film metallic Ag, it is possible to create *wiring* on regions that are initially essentially non-conducting. We performed such a study early in our research into this technique [40] and the results are briefly summarized here. This work involved a 50 nm thick Ag-doped sulfide electrolyte on a thick oxide layer on silicon substrates, patterned into channels with large Ag contacts (100 × 100 μm) at the ends. The 'off' resistance, R_{off}, was a geometric function of the channel dimensions, following:

$$R_{off} = \rho L/dW + R_p, \quad (5)$$

where ρ is the resistivity of the layer (in the mid 10^2 Ω cm range) and d the thickness of the chalcogenide, L is the channel's length, W is the channel's width and R_p is the effective resistance at zero channel length and is mainly due to electrode polarization (in the 10^8 to the low 10^9 Ω range for the electrode configuration used). A 10 × 10 μm device therefore exhibited an R_{off} around 1.5 GΩ. Fig. 8 shows the results from a number of 10 μm wide devices for programming, using a 5 s voltage sweep from 0.5 to 1.8 V with a 25 mA current limit. This produces a substantial surface electrodeposit with a resistance of around 1 Ω/μm of device length. The average contact resistance in this case is around 9 Ω.

5.4. Resonant frequency alteration

In situ frequency control of high Q microelectromechanical resonators is desirable as it is difficult to make structures that have an accurately defined and maintainable resonant frequency due to nanoscale material/processing irregularities and environmental factors (oxidation, condensation, etc.). We have demonstrated a tunable MEMS resonator using our electrolyte-electrodeposit system [3], shown schematically in Fig. 9(a). The resonator testbed is actually a set of 1 μm thick suspended polycrystalline silicon beams, ranging from 50 to 200 μm in length, with an 80 nm thick film of Ag–Ge–Se (sub-saturated) electrolyte on their top surface. A silver electrode is formed at one end and both ends have aluminum pads added to facilitate bonding/packaging for electrical characterization. The electrodeposit is made to form on the beam to change both its vibrating mass and stiffness. For testing, the packaged devices were placed on a piezoelectric chuck and their resonant frequency and Q-factor measured with the aid of a laser vibrometer before and after electrodeposition at 1.5 V. The results for a 150 μm long beam with a resonant frequency of 343 kHz are shown in Fig. 9(b) and indicate a frequency change of −3.27%, with an accompanying reduction in Q-factor from 3300 to 1600 due to damping, for the electrodeposition conditions used.

5.5. Control of surface wetting/valving

We have demonstrated that surface electrodeposition can be used to control wetting, increasing water contact angle by over 20°, and that this in turn can be used to regulate fluid flow through microchannels [7,41]. We fabricated a *microvalve* testbed by etching a 200 μm wide 20 μm deep microchannel with inlet and outlet reservoirs in silicon substrates as shown in Fig. 10(a). The channel was coated with a 50 nm thick Ag–Ge–Se solid electrolyte and Ag and Ni electrodes placed at a point between the reservoirs. A 10 V bias was sufficient to produce extended electrodeposit growth across the channel between the electrodes, as shown in Fig. 10(b), which is a scanning electron

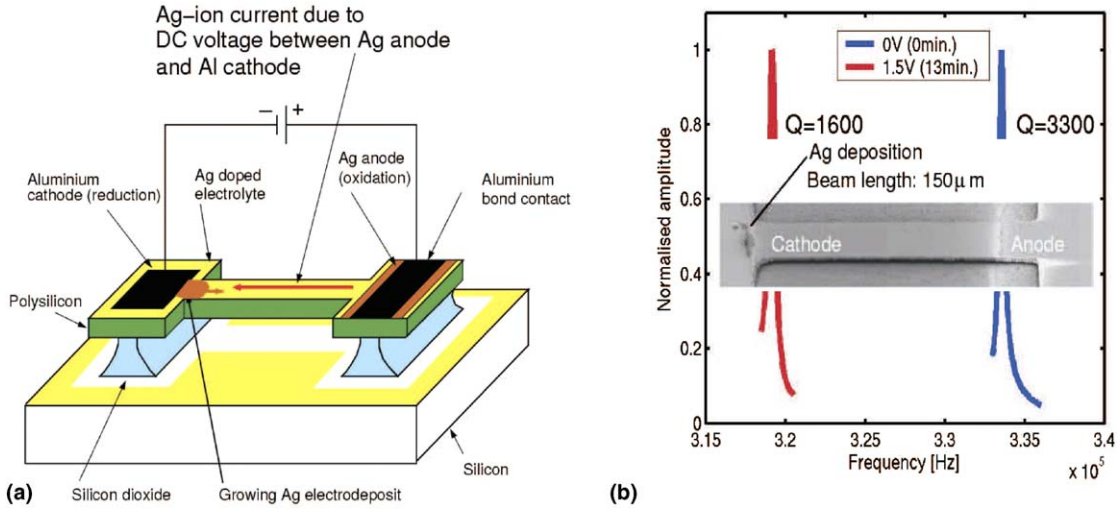

Fig. 9. (a) Schematic of a single suspended beam test structure; (b) effect of electrodeposition on resonant frequency and Q-factor for a 150 μm long beam following 1.5 V bias for 13 min (the inset is an electron micrograph of the structure following electrodeposition).

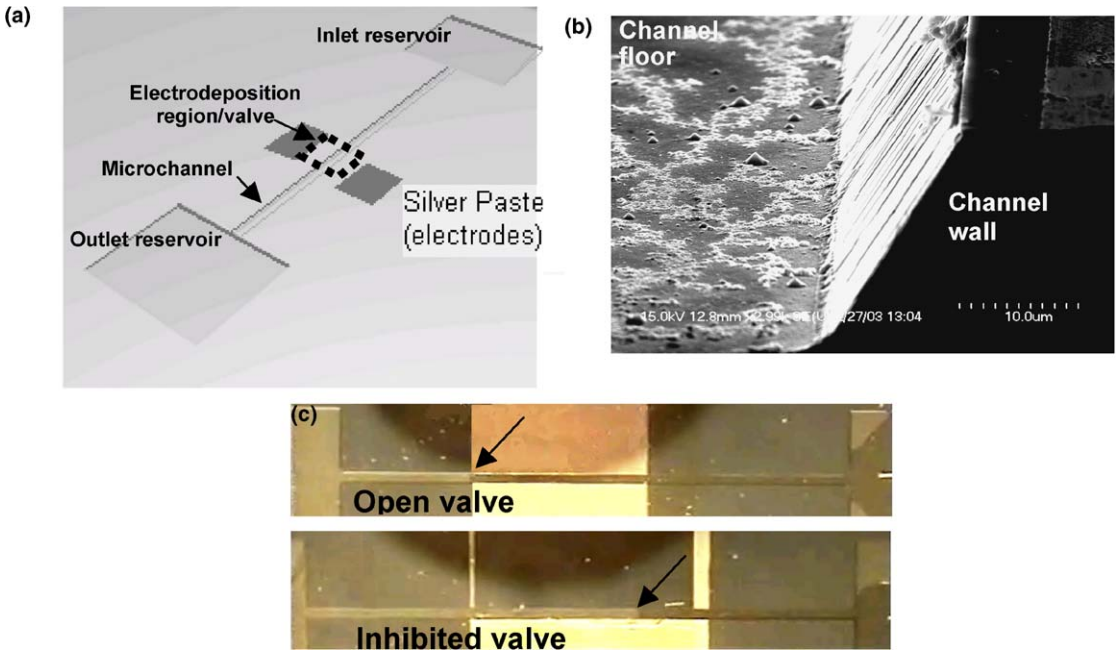

Fig. 10. (a) Schematic of testbed showing 'microvalve' between control electrodes; (b) scanning electron micrograph of electrodeposit on channel floor and wall. The bright features are the Ag electrodeposits; (c) demonstration of valving of pressure-driven flow in a microchannel. Top micrograph is the open valve after 6 s of flow and the bottom micrograph the inhibited valve after 35 s of flow in the valve region (6 s delay from inlet to valve edge in both cases). The arrows mark the position of the fluid front.

micrograph of an electrodeposit on the channel floor and wall. The bright features are the Ag electrodeposits and the sloping wall of the channel is due to the anisotropic etch. The electrodeposited Ag, which has a high surface area fractal structure less than 1 μm high, changes the fluid–surface interaction since fluid flow in a microchannel is dominated by the nature of the channel surface. This increase in effective hydrophobicity can be used to control the movement of the fluid. Fig. 10(c) illustrates pressure driven DI water flow for open (no electrodeposit) and inhibited (electrodeposit grown) valves 6 s after the fluid enters the valve region (12 s total flow time in the channel). As may be seen by the position of the markers (arrow), the flow has progressed to the outlet end of the valve in this time and continues to flow, eventually filling the reservoir. In the inhibited valve case, in which the electrodeposit has been grown across the channel using the conditions described above, after 6 s of flow in the channel from the inlet, the fluid front stops abruptly at the front edge of the valve region, demonstrating valving action.

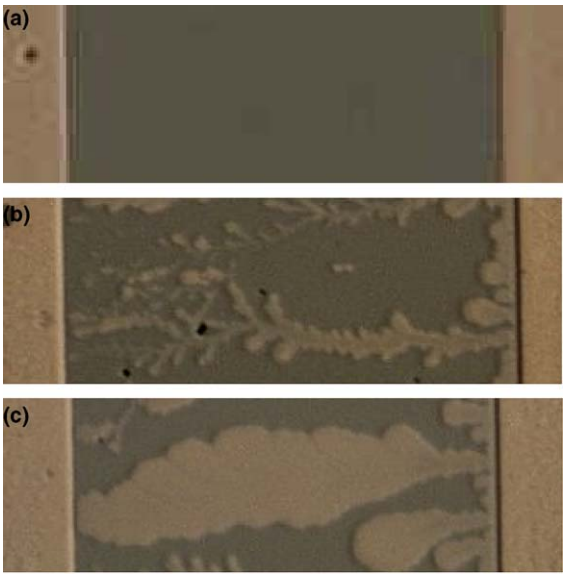

Fig. 11. (a) Clear 50 μm wide (between the light-colored metal electrodes) element prior to application of bias; (b) dendritic Ag electrodeposit grown in element which reflects about 20% of incident light; (c) broad electrodeposit, which reflects about 60% of incident light.

5.6. Alteration of reflectance

Surface electrodeposition can be used to alter the reflectance of a surface as the optical properties of the metal are obviously radically different from those of the electrolyte film. To demonstrate this, we created solid electrolyte (50 nm thick Ag–Ge–Se) patterns on thick oxide grown on silicon wafers, with wide electrodes at either end (Ag and Ni). Before the application of a bias, the light is able to pass through the thin film to be reflected by the substrate with little impediment, as shown in Fig. 11(a). After the electrodeposit has been formed, the light is blocked/reflected from the grown metallic surface. Two examples are given in Fig. 11(b) and (c) for 20% and 60% coverage respectively [42]. These elements can be potentially used as optical switches.

6. Conclusions

We have shown that the addition of a metal such as Ag to a thin film of germanium chalcogenide base glass by photodissolution creates a nano-phase separated material with unique and useful characteristics. The ternaries formed by photodissolution of metal from a surface film are solid electrolytes, by virtue of the presence of a dispersed superionic nanocrystalline phase, that are stable over a wide range of operating temperatures. These materials can be used to transfer mass by oxidation of a metal source and reduction of the metal ions at a supply of electrons and that this effect leads to new functionality of the glasses. We have demonstrated several of these new functions, the most significant being solid state non-volatile memory elements that switch rapidly at very low voltage and current between widely spaced resistance states and possess excellent cycling characteristics. We have also shown the utility of the technique in 'programmable' wiring in integrated circuits, the tuning of microelectromechanical resonators, the control of fluid flow in microchannels, and the control of light transmission/reflection in optical elements. Such diversity of applications suggests that these materials could very well play a large part in a wide range of future technologies and are therefore deserving of continued study.

Acknowledgements

This work was sponsored by Axon Technologies Corp. The authors would like to acknowledge the invaluable contributions of J. Aberouette, P. Maroufkhani, M. Park, C. Gopalan, M. Balakrishnan, T.L. Alford and H.C. Kim to the experimental research described in this review.

References

[1] W.C. West, K. Sieradzki, B. Kardynal, M.N. Kozicki, J. Electrochem. Soc. 145 (1998) 2971.
[2] S.R. Forrest, T.A. Witten Jr., J. Phys. A 12 (1972) L109.
[3] S. Enderling, C.L. Brown III, M. Balakrishnan, J. Hedley, J.T.M. Stevenson, S. Bond, C.C. Dunare, A.J. Harris, J.S. Burdess, M. Mitkova, M.N. Kozicki, A.J. Walton, Technical Digest of the 18th IEEE Conference on Micro Electro Mechanical Systems (MEMS 2005), 2005, p. 159.
[4] M.N. Kozicki, M. Mitkova, J.P. Aberouette, Physica E 19 (2003) 161.
[5] M.N. Kozicki, M. Park, M. Mitkova, IEEE Trans. Nanotechnol. 4 (2005) 331.
[6] R. Symanczyk, M. Balakrishnan, C. Gopalan, T. Happ, M. Kozicki, M. Kund, T. Mikolajick, M. Mitkova, M. Park, C. Pinnow, J. Robertson, K. Ufert, in: Proceedings of the Non-Volatile Memory Technology Symposium, San Diego, CA, November 2003, p. 17.
[7] M.N. Kozicki, P. Maroufkhani, M. Mitkova, Superlattices Microstr. 34 (2004) 467.
[8] K. Terabe, T. Hasegawa, T. Nakayama, M. Aono, Nature 433 (2005) 47.
[9] T. Sakamoto, H. Sunamura, H. Kawaura, T. Hasegawa, T. Nakayama, M. Aono, Appl. Phys. Lett. 82 (2003) 3032.
[10] A. Antonaia, M.C. Santoro, G. Fameli, T. Polichetti, Thin Solid Films 426 (2003) 281.
[11] M.N. Kozicki, M. Mitkova, J. Zhu, M. Park, Microelectron. Eng. 63 (2002) 155.
[12] T. Kawaguchi, S. Maruno, S.R. Elliott, J. Appl. Phys. 79 (1996) 9096.
[13] M. Mitkova, Y. Wang, P. Boolchand, Phys. Rev. Lett. 83 (1999) 3848.
[14] Y. Wang, M. Mitkova, D.G. Georgiev, S. Mamedov, P. Boolchand, J. Phys.: Condens. Matter 15 (2003) S1573.
[15] P. Boolchand, F. Wang, U. Vempati, M. Mitkova, M. Kozicki, Bull. Am. Phys. Soc. 49 (2004) 826.
[16] T. Kawaguchi, S. Maruno, J. Appl. Phys. 71 (1992) 2195.
[17] K. Shimakawa, A. Kolobov, S.R. Elliott, Adv. Phys. 44 (1995) 475.
[18] P. Boolchand, in: P. Boolchand (Ed.), Insulating, Semiconducting Glasses, World Scientific, 2000, p. 214.
[19] N.V. Bondar, N.A. Davydova, V.V. Tishchenko, M. Vlcek, J. Mol. Struct. 555 (2000) 175.
[20] Y. Wang, K. Tanaka, T. Nakaokan, K. Murase, J. Non-Cryst. Solids 299–302 (2002) 963.
[21] M. Mitkova, M.N. Kozicki, J. Non-Cryst. Solids 299–302 (2002) 1023.
[22] A. Feltz, H. Aust, A. Pelyer, J. Non-Cryst. Solids 55 (1983) 190.

[23] X. Feng, W.J. Bresser, P. Boolchand, Phys. Rev. Lett. 78 (1997) 4422.
[24] P. Boolchand, D.G. Georgiev, T. Qu, F. Wang, L. Cai, S. Chakravarty, C. R. Chimie 5 (2002) 713.
[25] N.A. Davydova, V.V. Tishchenko, J. Baran, M. Vlchek, J. Mol. Struct. 450 (1998) 117.
[26] T. Wagner, A. Macková, V. Peřina, E. Rauhala, A. Seppälä, S.O. Kasap, M. Frumar, Mir. Vlček, Mil. Vlček, J. Non-Cryst. Solids 299 (2002) 1028.
[27] A.V. Kolobov, S.R. Elliott, Adv. Phys. 40 (1991) 625.
[28] J.H.S. Rennie, S.R. Elliott, J. Non-Cryst. Solids 97&98 (1987) 1239.
[29] A.V. Kolobov, S.R. Elliott, M.A. Taguirdzhanov, Philos. Mag. B 61 (1990) 857.
[30] I.Z. Indutni, V.A. Danko, A.A. Kudryavtsev, E.V. Michailovskaya, V.I. Minko, J. Non-Cryst. Solids 185 (1995) 176.
[31] G. Kluge, Phys. Status Solidi (a) 101 (1987) 105.
[32] A.V. Kolobov, G.E. Bedel'baeva, Philos. Mag. B 64 (1991) 21.
[33] P. Boolchand, W. Bresser, Philos. Mag. B 80 (2000) 1757.
[34] J. Fick, B. Nicolas, C. Rivero, K. Elshot, R. Irwin, K.A. Richardson, M. Fisher, R. Vallee, Thin Solid Films 418 (2002) 215.
[35] T. Akai, S.W. Martin, F. Borsa, Phys. Rev. B 63 (2001). Art. No. 024303.
[36] M.N. Kozicki, C. Gopalan, M. Balakrishnan, M. Park, M. Mitkova, in: Non-Volatile Memory Technology Symposium Orlando, FL USA, 15–19 November 2004.
[37] M.N. Kozicki, S.W. Hsia, A.E. Owen, P.J.S. Ewen, J. Non-Cryst. Solids 137&138 (1991) 1341.
[38] M.N. Kozicki, US Patent 6,469,364, 2002.
[39] M.N. Kozicki, M. Mitkova, US Patent 6,635,914, 2003.
[40] M.N. Kozicki, M. Yun, L. Hilt, A. Singh, in: E.D. Wachsman et al. (Eds.), Proceedings of the 1999 Symposium on Solid State Ionic Devices, The Electrochemical Society, 1999, p. 1.
[41] M.N. Kozicki, P. Maroufkhani, M. Mitkova, in: Proceedings of Nanotech 2005, NSTI, Anaheim, CA, May 2005.
[42] J.P. Aberouette, Masters thesis, Arizona State University, 2002.